

Check for updates

www.afm-journal.de

# Tetragonal Kondo Insulator EuCd<sub>2</sub>Sb<sub>2</sub> Discovered via High Pressure High Temperature Synthesis

Jose L. Gonzalez Jimenez, Corey Melnick, Krishna Prasad Koirala, Ran Adler, Fei Wang, Meryem Berrada, Bin Chen, Le Wang, David Walker, Gabriel Kotliar, and Weiwei Xie\*

Magnetic and electronic properties of quantum materials heavily rely on the crystal structure even in the same chemical compositions. In this study, it is demonstrated that a layered tetragonal  $EuCd_2Sb_2$  structure can be obtained by treating bulk trigonal  $EuCd_2Sb_2$  under high pressure (6 GPa) and high temperature (600 °C). Magnetization measurements of the newly formed layered tetragonal  $EuCd_2Sb_2$  confirm an antiferromagnetic ordering with Neel temperature ( $T_N$ ) around 16 K, which is significantly higher than that ( $T_N\approx 7$  K) of trigonal  $EuCd_2Sb_2$ , consistent with heat capacity measurements. Moreover, bad metal behavior is observed in the temperature dependence of the electrical resistivity and the resistivity shows a dramatic increase around the Neel temperature. Electronic structure calculations with local density approximation dynamic mean–field theory (LDA+DMFT) show that this material is strongly correlated with well-formed large magnetic moments, due to Hund's coupling, which is known to dramatically suppress the Kondo scale.

1. Introduction

Magnetic semiconductors are characterized by lattices composed of magnetic atoms. Recently, magnetic topological semiconductors, one kind of intrinsic magnetic semiconductor, have attracted interest in condensed matter physics because of various quantum phenomena, such as axion insulators and anomalous Hall effects. Currently, the study of such systems in bulk materials primarily focuses on Mn-based and Eubased intrinsic magnetically ordered topological insulators that can directly affect the topological properties by introducing magnetic symmetries.<sup>[1-5]</sup> Among them, YbMnBi<sub>2</sub>[3] was theoretically proposed and experimentally confirmed to be a magnetic topological insulator in which band topology from Bi square nets and magnetism from Mn<sup>2+</sup> interplay. Later the family of compounds,  $(MnTe)_n (Bi_2 Te_3)_m [4-7]$ with a natural heterostructure of MnTe and Bi<sub>2</sub>Te<sub>3</sub> layers, was discovered and investigated. The band topology is attributed to Bi<sub>2</sub>Te<sub>3</sub> layers, whereas magnetism is contributed from MnTe layers. Meanwhile, an increasing number of Eu-based intrinsic magnetic compounds were identified and

investigated in search of band topology induced by broken time-reversal symmetry. Such examples include the antiferromagnetic topological insulators  $EuCd_2As_2^{[8-10]}$  and  $EuIn_2As_2^{[11]}$  Recently, a new family of compounds, trigonal  $EuM_2Pn_2$  (M = Mg<sup>2+</sup>, Mn<sup>2+</sup>, Zn<sup>2+</sup>, and Cd<sup>2+</sup>; Pn = P<sup>3-</sup>, As<sup>3-</sup>, Sb<sup>3-</sup>, and Bi<sup>3-</sup>), was studied for the interplay of magnetism and band topology, such

J. L. G. Jimenez, W. Xie
Department of Chemistry
Michigan State University
East Lansing, MI 48824, USA
E-mail: xieweiwe@msu.edu
C. Melnick, G. Kotliar
Condensed Matter Physics and Materials Science Department
Brookhaven National Laboratory
Upton, NY 11973, USA
K. P. Koirala, L. Wang
Physical and Computational Sciences Directorate
Pacific Northwest National Laboratory
Richland, WA 99354, USA
The ORCID identification number(s) for the author(s) of this article

can be found under https://doi.org/10.1002/adfm.202303612
© 2023 The Authors. Advanced Functional Materials published by
Wiley-VCH GmbH. This is an open access article under the terms of the
Creative Commons Attribution-NonCommercial-NoDerivs License,
which permits use and distribution in any medium, provided the original
work is properly cited, the use is non-commercial and no modifications

DOI: 10.1002/adfm.202303612

R. Adler, G. Kotliar
Physics Department and Center for Materials Theory
Rutgers University
Piscataway, NJ 08854, USA
F. Wang
Department of Chemistry and Biochemistry
Missouri State University
Springfield, MO 65897, USA
M. Berrada, B. Chen
Hawai'i Institute of Geophysics and Planetology
University of Hawai'i at Mānoa
Honolulu, HI 96822, USA

D. Walker Lamont Doherty Earth Observatory Columbia University Palisades, NY 10964, USA

or adaptations are made.

www.advancedsciencenews.com



www.afm-journal.de

as  $\operatorname{EuMg_2Bi_2},^{[12,13]}$   $\operatorname{EuMn_2P_2},^{[14]}$  and  $\operatorname{EuCd_2Sb_2},^{[15,16]}$  Moreover, breaking the spatial inversion symmetry (P), which can be tuned through the distortion of the lattice by high pressure compression, or time-reversal symmetry (T) in the form of a paramagnetic to antiferromagnetic state transition, can split the Dirac point into a pair of Weyl points in topological materials. [13] The P-breaking Weyl fermions can be realized by forming noncentrosymmetric crystal structures, for example TaAs [17–20] and (W/Mo)Te<sub>2</sub>. [21–26] T-breaking approach was proposed to occur with a spontaneous magnetism to break T, for example, in trigonal 122-EuCd<sub>2</sub>Sb<sub>2</sub>. [15] In trigonal EuCd<sub>2</sub>Sb<sub>2</sub>, A-type AFM structure hosts in-plane magnetic moments on Eu atoms that form FM layers stacking antiferromagnetically along the *c*-axis with the antiferromagnetic transition temperature  $\approx 7$  K. [15]

On the other hand, Eu-intermetallic compounds such as  ${\rm EuPd_2Si_2}^{[27]}$  are famous for bivalent and other strong correlated system properties such as potential heavy fermions. However, those 122-phases always adopt the tetragonal structures and their derivates. Our previous high pressure work on trigonal 122-type phases[<sup>28]</sup> has indicated that the trigonal  ${\rm La_2O_3}$  structure could undergo structural transition at high pressure, for example,  ${}^{\sim}3$  GPa in  ${\rm CaMn_2Bi_2}$ . The high pressure can be used to tune the atomic distances and crystal structures to induce unexpected quantum phenomena such as superconductivity, metal-to-insulator transition (MIT), and so on. Thus, we were inspired to tune the magnetic topological materials into heavy fermion compounds. To achieve this, we applied high pressure and high temperature treatment to the rare-earth based magnetic topological material,  ${\rm EuCd_2Sb_2}$ .

Herein, we report the synthesis and characterization of the new magnetic semiconductor, EuCd<sub>2</sub>Sb<sub>2</sub>, with a tetragonal layered structure. EuCd<sub>2</sub>Sb<sub>2</sub> adopted a tetragonal structure from the original trigonal structure, as determined by both X-ray diffraction and electron diffraction in the transmission electron microscope (TEM), following treatment at high pressure of 6 GPa and high temperature of 600 °C for 24 h. We observed an antiferromagnetic transition around 16 K. The electrical resistance measurement shows an increase in resistance with decreasing temperature, consistent with bad metal properties. At low temperatures around AFM transition temperature, the resistance increases dramatically. To confirm this, the low-temperature heat capacity on tetragonal EuCd<sub>2</sub>Sb<sub>2</sub> was measured with Sommerfeld parameter,  $\gamma$ , over 0.33(2) J mol<sup>-1</sup>-K<sup>-2</sup>, which indicates EuCd<sub>2</sub>Sb<sub>2</sub> is potentially a heavy-fermion Kondo insulator candidate. Such kind of changes can be induced by the interplay between Kondo effects and magnetic contribution.

## 2. Results and Discussion

A new tetragonal  $EuCd_2Sb_2$  structure was detected in the product synthesized at 6 GPa and 600 °C. The space group and lattice parameters were determined by indexing the powder X-ray diffraction pattern. The high pressure and high temperature product of  $EuCd_2Sb_2$  crystallized in tetragonal structure type with the space group P4/mmm. However, the reflections from  $EuCd_2Sb_2$  by single crystal X-ray diffraction are weak enough to require independent confirmation. To confirm the phase information, we combined powder X-ray diffraction and selected area electron diffraction to assist the structural determination based on the

space group and lattice parameters generated from single crystal X-ray diffraction. The powder diffraction pattern (Figure 1a) can be successfully indexed, and cell parameters were refined using the ones obtained from single crystal X-ray diffraction experiments. The refinement based on powder diffraction shows tetragonal lattice parameters for EuCd<sub>2</sub>Sb<sub>2</sub> (Figure 1b) adopts the CeMg<sub>2</sub>Si<sub>2</sub> structure type, a derivative of the more commonly known ThCr<sub>2</sub>Si<sub>2</sub> structure, [29] as opposed to the reported ambient pressure precursor, which adopts the CaAl<sub>2</sub>Si<sub>2</sub> structure. To confirm the lattice parameters and unit cells, the high pressure EuCd<sub>2</sub>Sb<sub>2</sub> was investigated by electron microcopy. The experimental and simulated electron diffraction patterns taken along [100] zone axis (Figure 1c,1d) allow the determination of the dspacing ( $\approx$ 5.67 Å) of the crystallographic *c*-axis with errors. Additional information on the chemical composition and structural analysis can be found in Figures S1,S2 (Supporting Information).

To get insight into the magnetic properties and compare them to the reported trigonal EuCd<sub>2</sub>Sb<sub>2</sub>, we performed temperaturedependent magnetization measurements on the high pressure polycrystalline sample of tetragonal EuCd<sub>2</sub>Sb<sub>2</sub> at a low applied field (0.1 T) from 2 to 300 K. The results are shown in Figure 2 (a). A magnetic transition to an antiferromagnetic state  $(T_N)$  is observed at around 16 K. The reported trigonal EuCd<sub>2</sub>Sb<sub>2</sub> shows an antiferromagnetic order only around 7 K.[15] The magnetic susceptibility decreases below the  $T_N$  slightly, which is much smaller than the regular antiferromagnetic ordering. Similar magnetic properties were detected in other Eu-based compounds, such as EuIn2As2, which also indicates helical magnetic ordering in tetragonal EuCd<sub>2</sub>Sb<sub>2</sub>.<sup>[11]</sup> At temperatures higher than 16 K, classic Curie-Weiss behavior is observed. The effective moment and Curie-Weiss (CW) temperature were fitted from 25 to 50 K by using Curie-Weiss law in Figure S3. The Curie-Weiss temperature fitted ranging from 25 K to 300 K is -7.5 (5)(7 K, while the average effective moment is 8.05 (2)  $\mu_{\rm B}$ /Eu, which is slightly larger than the theoretical effective moment of Eu<sup>2+</sup> (7.94  $\mu_{\rm B}$ ). The magnetic characteristics above  $T_N$  are essentially isotropic. The temperature below 10 K, where the field-cooled (FC) and zero-field-cooled (ZFC) curves differ, is usually associated with a blocking temperature ( $T_{\rm B}$ ) related to the domain of larger particle size in the sample. Usually, the whole sample becomes super-paramagnetic/ferromagnetic above the blocking temperature. The peak in the ZFC curve at around 6 K is usually ascribed to an average  $T_{\rm B}$  associated with the average particle size in the distribution. The field-dependent behavior is characteristic of an antiferromagnetic material with a mixture of ferromagnetic or super-paramagnetic components. The magnetic moment of tetragonal EuCd<sub>2</sub>Sb<sub>2</sub> reaches about 4.84  $\mu_B$ /Eu for applied fields up to 9 T at 2 K, as shown in Figure Figure 3. Moreover, the non-linear field-dependent magnetization at 2 K is also consistent with the other magnetic interactions, possibly a superparamagnetic/ferromagnetic ordering and antiferromagnetic or-

The temperature-dependent resistivity for a piece of tetragonal  $EuCd_2Sb_2$ , measured from 2 to 300 K, is shown in Figure 4 (main panel). The resistivity increases with decreasing the temperature (semiconducting behavior). The temperature decreases from 300 to 100 K while the resistivity starts increasing because covalent bonds start breaking and the majority carrier decreases. Arrhenius line fitting of the resistivity data at high temperature

1616328, 0, Downloaded from https://onlinelibrary.wiley.com/doi/10.1002/adfm.202303612, Wiley Online Library on [25/082023]. See the Terms and Conditions (https://onlinelibrary.wiley.com/terms-and-conditions) on Wiley Online Library for rules of use; OA articles are governed by the applicable Creative Commons License

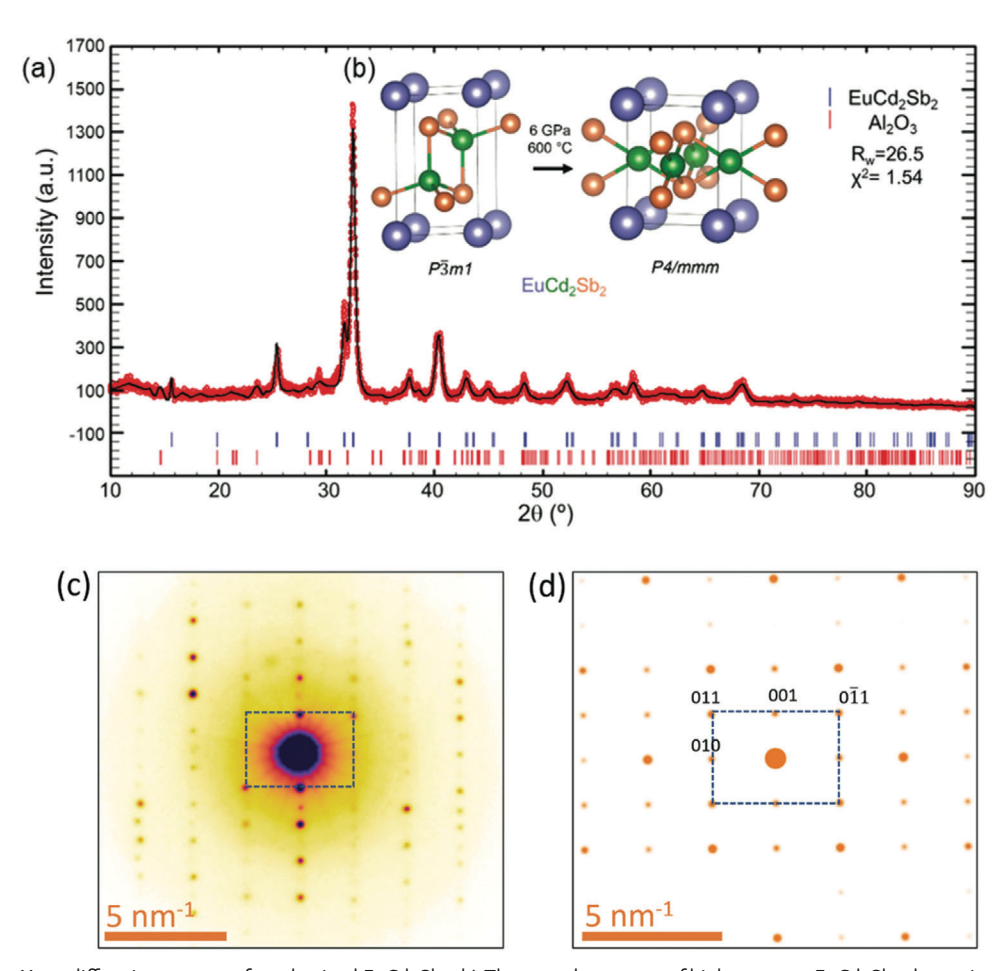


**Figure 1.** a) Powder X-ray diffraction pattern of synthesized EuCd<sub>2</sub>Sb<sub>2</sub>. b) The crystal structure of high pressure EuCd<sub>2</sub>Sb<sub>2</sub> determined by a combination of X-ray diffraction and TEM (Eu: purple, Cd: green, Sb: orange). c). Experimental and d) simulated electron diffraction patterns of EuCd<sub>2</sub>Sb<sub>2</sub> along [100] zone axis.

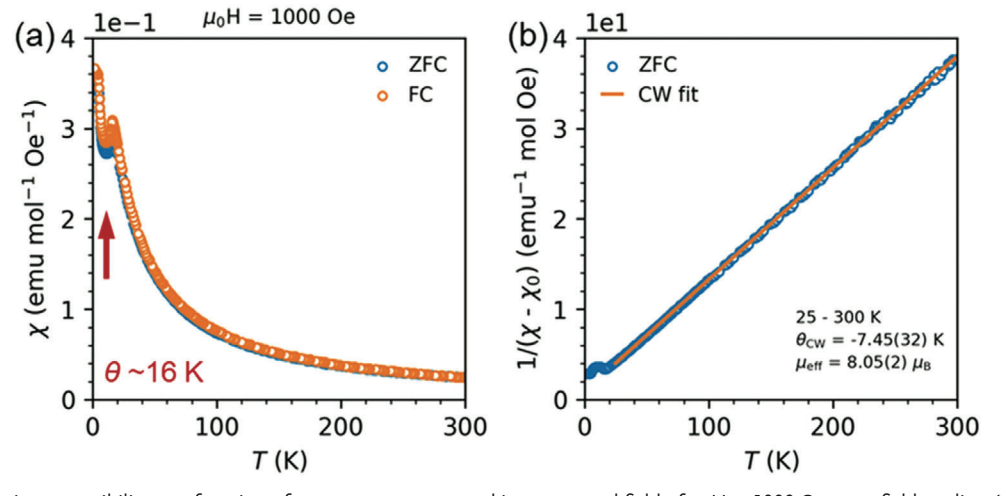


**Figure 2.** a) Magnetic susceptibility as a function of temperature measured in an external field of  $\mu_0$ H = 1000 Oe, zero-field cooling (ZFC) mode (blue) and field cooling (FC) mode (orange). b) Curie–Weiss fitting of the magnetic susceptibility from 25 to 300 K.



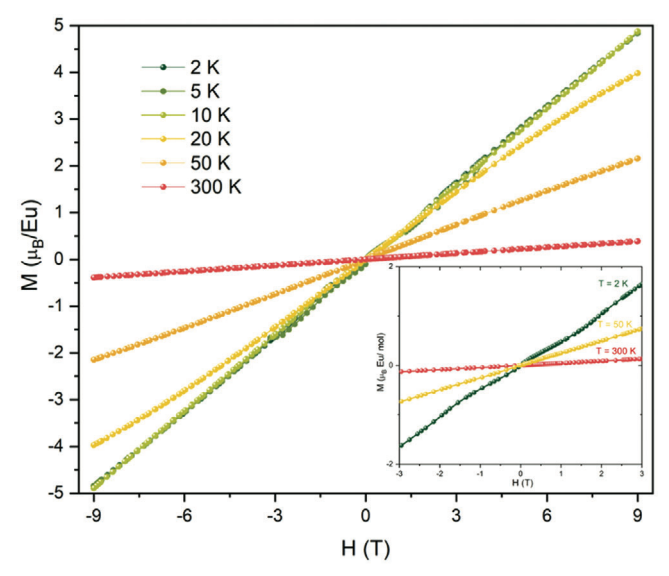


**Figure 3.** The field-dependent magnetization for the sample measured at various temperatures from 2–300 K with the applied field up to 9 T. (Inset) The field-dependent magnetization from -3 to 3 T with the emphasis of the non-linear field-dependent magnetization at 2 K.

range (190–200 K) further reveals the bandgap of approximately 0.06 eV with an activation energy of  $\approx$ 23 meV. Usually, the charge transport is sensitive to the magnetic state of the system: the resistivity shows a dramatic increase below the Neel temperature ( $\approx$ 16 K). Such a dramatic increase in resistivity might indicate the possibility of a Kondo insulator of tetragonal EuCd<sub>2</sub>Sb<sub>2</sub>. To test the possibility of Kondo insulating occurring in the resistivity around16 K, the electronic structures of EuCd<sub>2</sub>Sb<sub>2</sub> and hypothetical "SrCd<sub>2</sub>Sb<sub>2</sub>" in the same structure were calculated. For EuCd<sub>2</sub>Sb<sub>2</sub>, the calculation includes the effects of on-site Coulomb

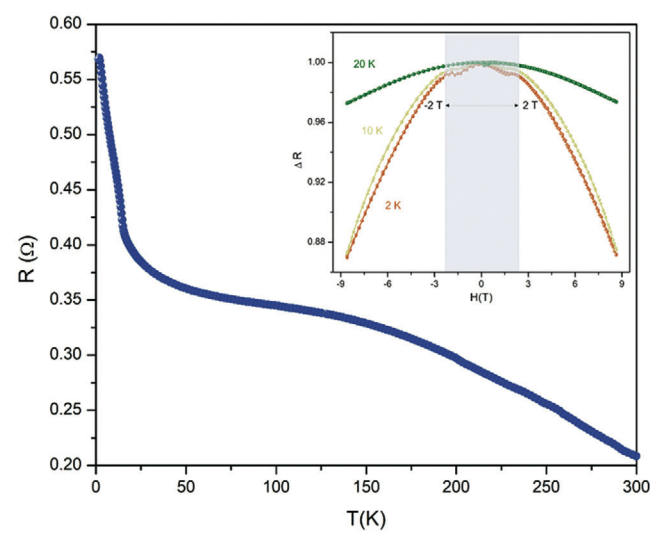


**Figure 4.** (Main Panel) Temperature-dependent resistance measured between 1.8 and 300 K in the applied magnetic field of 1T. (Inset) Field-dependence of the resistance at various temperatures (2, 10, and 20 K) with applied field from -9 to +9 T normalized to the values at 0 applied magnetic field.

interaction (U) with U = 4.5 eV applied on Eu 4f electrons. The relativistic spin-orbit coupling (SOC) was considered in both compounds. It is clearly shown that SrCd<sub>2</sub>Sb<sub>2</sub> and EuCd<sub>2</sub>Sb<sub>2</sub> share similar band structures around Fermi level (see Figures S7 Supporting Information), which indicates the semiconductorinsulator transition observed in EuCd<sub>2</sub>Sb<sub>2</sub>may relate to the magnetic transition, instead of being induced from Kondo effects. The bandgap opens up ≈16 K which likely results from hybridization of localized f-electrons in Eu atoms with conduction electrons. As a consequence, a transition from semiconducting behavior to insulating behavior at ≈16 K is seen in resistivity measurements. Moreover, the magnetoresistance of tetragonal EuCd<sub>2</sub>Sb<sub>2</sub> was measured at various temperatures from -9 to +9 T. At low temperatures (2 K), the material's resistance slightly increases and then decreases, eventually forms a domelike magneto-resistance feature when the magnetic field is applied. At 2 K, it decreases by ≈14% when the field increased from 0 to 9 T. This behavior is consistent with the anomalous magnetoresistance seen in magnetic spin-flop systems. However, compared to the magneto-resistivity in trigonal EuCd<sub>2</sub>Sb<sub>2</sub> at ambient pressure that shows the chiral magnetic effect at the low field range (-0.5-+0.5 T), [16] the magneto-resistivity in tetragonal EuCd<sub>2</sub>Sb<sub>2</sub> doesnot show similar electrical phenomena (Figure 4 Inset).

The lambda-shape anomaly observed in the heat capacity measurement presented in Figure 5 at  $T_{\rm N}\approx 16$  K without applying an external magnetic field indicates a second–order phase transition in tetragonal EuCd<sub>2</sub>Sb<sub>2</sub>, which is in good agreement with the antiferromagnetic transition observed in the magnetic susceptibility and entropy curve found in Figures S1,S7 (Supporting Information). Without including the magnetic contribution, the electronic contribution ( $\gamma$ T), and phonon contribution ( $\beta$ T³) are the major parts of the specific heat. To further confirm the possibility of heavy fermion properties in tetragonal EuCd<sub>2</sub>Sb<sub>2</sub>, the specific heat was fitted with the equation:  $C_{\rm p}/{\rm T}=\gamma+\beta{\rm T}^2$ . The Sommerfeld coefficient ( $\gamma$ ) is 0.33(2) J mol<sup>-1</sup>-K<sup>-2</sup>, which is smaller than that of reported heavy fermion compound CeCoIn<sub>5</sub>, [<sup>30]</sup> but significantly larger than that of regular metals for which heavy fermion theory was first used for (**Figure 5** Inset).

There are two limiting cases for the behavior of Kondo systems, in one limit the Kondo effect takes place, in the other limit, the RKKY effect dominates, the Kondo effect does not take place, and the system orders magnetically. The atomic physics of the Europium also has two limits: 1) The spin-orbit coupling dominates over the Hund's coupling, such that the J = 5/2 subshell is filled with six electrons and the remaining electron fluctuates between (or selects one of) the remaining eight I = 7/2 electron states; 2) the Hund's coupling dominates the spin orbit coupling and Hund's physics emerges.<sup>[31]</sup> That is, the f-electron spins align, the electrons half-fill the f-shell, the correlated electrons experience a very large effective Hubbard interaction,  $U_{eff}$ , and, in the paramagnetic state, the f electrons form upper and lower Hubbard bands. In case (1), the Kondo physics emerges at reasonable temperatures. In case (2), the Kondo scale is miniscule. Here we perform DFT+DMFT calculations of tetragonal EuCd<sub>2</sub>Sb<sub>2</sub> at 300 K within Portobello<sup>[32]</sup> with a 2.5 eV Hubbard interaction (U), a 0.5 eV Hund's coupling (I), and the nominal double counting with half-filling of the f-shell (N = 7). The results are consistent with case (2), as shown in Figure 6, and remain consistent

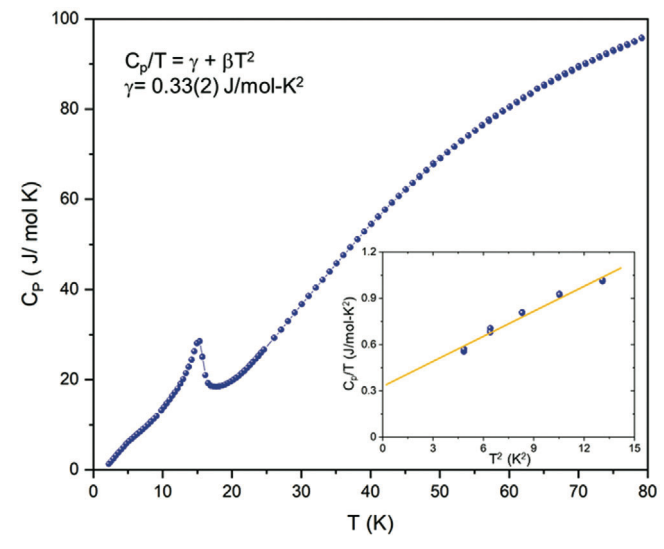


**Figure 5.** (Main Panel) Temperature-dependent heat capacity  $C_p(T)$  in tetragonal  $EuCd_2Sb_2$  without applied field. (Inset) The specific heat fitting includes the electron and phonon contributions.

provided the Hund's coupling is greater than  $\approx 0.2$  eV. Indeed, the gap between the upper and lower Hubbard band is approximately  $U_{\rm eff} = U + (N-1)J = U + 6J$ , exactly as expected in case (2) .<sup>[31]</sup> DFT, in contrast, cannot include the many-bodied physics of the Hund's coupling and therefore defaults to case (1), as shown in Figure 6. This is also consistent with the experimental results, the large magnetic moment of slightly of over 8  $\mu_{\rm B}$  suggests that the Eu-f shell is completely spin-polarized (with the remaining moment comes from a very small contribution of the conduction electrons). The presence of magnetic moments at high temper-

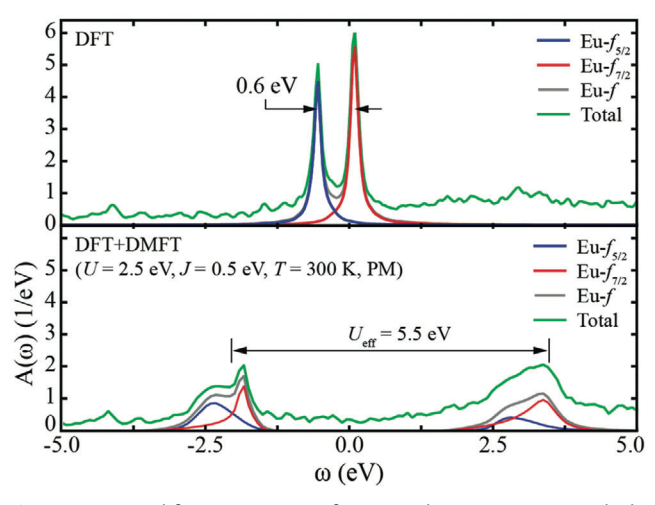


**Figure 6.** Spectral functions, A( $\omega$ ), of tetragonal paramagnetic EuCd $_2$ Sb $_2$  as predicted by DFT and DFT+DMFT. DFT places the Eu-f shell very near the chemical potential, with the J=7/2 states lying on the Fermi surface and the J=5/2 split (by the spin-orbit coupling)  $\approx$ 0.6 eV below the chemical potential. DFT+DMFT, in contrast, predicts that the Hund's coupling aligns spins in the half-filled Eu-f shell and are driven far from the Fermi surface by a large effective Hubbard interaction. This behavior is insensitive to the choice of U and J, provided J>0.2 eV and  $U_{eff}>5$  eV.

atures accounts for the bad metal behavior observed in the resistivity, which is different from the Weyl semimetal behavior in trigonal EuCd<sub>2</sub>Sb<sub>2</sub>. Below the magnetic transition, the resistivity increases as the magnetism reconstructs the Fermi surface.

#### 3. Conclusion

In summary, we reported the high pressure and high temperature synthesis, structural characterization, and magnetic and specific heat measurements on  $EuCd_2Sb_2$ . The crystal structure changes from trigonal to tetragonal symmetry after being treated under high pressure and high temperature. The antiferromagnetic transition temperature increases from  $\approx\!\!7$  K in trigonal symmetry to 16 K in tetragonal symmetry. Susceptibility measurements and the Lambda-shaped anomalies in the specific heat are consistent with a magnetic transition. Charge self-consistent DFT+DMFT simulations predict that the Kondo scale is dramatically suppressed by the Hund's coupling and therefore supports the picture of the phase transition due to a magnetic transition.

## 4. Experimental Section

Synthesis: Ambient pressure EuCd<sub>2</sub>Sb<sub>2</sub> was obtained by mixing a stoichiometric ratio (1:2:2) of europium pieces (Alfa Aesar, sublimed dendric, 99.9%), cadmium shot (Alfa Aesar, 99.999%), and powdered antimony (Alfa Aesar, 99.5%). The mixture with the total mass 300 mg was pressed into an 1/4-inch diameter pellet, put into an alumina crucible, and then sealed inside the evacuated quartz tube (<  $10^{-5}$  Torr). The tubes were heated to 1000 °C at the speed of 60 °C h<sup>-1</sup>, heated at 1000 °C for 24 h, followed by cooling to room temperature at a rate of 100 °C  $h^{-1}$ . The highpressure sample was obtained by grinding crystals of the ambient condition EuCd<sub>2</sub>Sb<sub>2</sub> product into a powder and placing it inside an Al<sub>2</sub>O<sub>3</sub> crucible that was inserted into an 8 mm Cermacast 646 octahedral pressure medium lined with a steel foil heater. The sealed sample was then compressed to 6 GPa (290 tons)[33] in a Walker-type multi-anvil press. Afterward, the sample was heated to 600 °C and kept for 25 h. The sample, indexed as TT-1447, was quenched at pressure by cutting heater power and depressurizing overnight.

Structure Determination and Phase Analysis: To determine the structure of the high pressure EuCd<sub>2</sub>Sb<sub>2</sub> product, single crystals were examined at room temperature via a Bruker D8 Quest Eco single-crystal X-ray diffractometer using Mo radiation ( $\lambda_{\rm K}\alpha=0.71073$  Å). Measurement parameters include a scan width( $\omega$ ) of 1.0° and an exposure time of 10 s per frame. The SMART software was used for data acquisition. Intensities were extracted and corrected for Lorentz and polarization effects using the SAINT program. The unit cell and space group information was obtained from the single crystal X-ray diffraction. The high-pressure product was also ground for powder diffraction using Bruker D2 Phaser powder X-ray diffractometer with Cu K $\alpha$  radiation ( $\lambda = 1.5460$  Å). A step size of 0.004 ° at a scan speed of 0.55 °min<sup>-1</sup> was used to measure a spectrum over a Bragg angle (2 $\theta$ ) range of 10–90° using a Bruker silicon low background sample holder. Powder data was refined through the LeBail method using the FullProf software according to the unit cell and space group obtained from single crystal X-ray diffraction data. To confirm the lattice parameters in the unit cell, thin samples were examined for selected area electron diffraction (SAED) by using a JEOL 7500F scanning transmission electron microscope (STEM).

Chemical Compositions Characterization: Elemental composition within the samples was determined by energy dispersive X-ray spectroscopy (EDS) in scanning electron microscope (SEM) [JEOL Ltd., Tokyo, Japan]. The EDS data were acquired and analyzed in an Oxford Instruments AZtec system (Oxford Instruments, High Wycomb, Bucks, England), software version 3.1 using a 20 mm² Silicon Drift Detector

**ADVANCED** SCIENCE NEWS

www.advancedsciencenews.com

ADVANCED FUNCTIONAL MATERIALS

www.afm-journal.de

(JEOL 6610LV SEM) and an ultra-thin window. Samples were mounted in epoxy, polished and then sputter coated with thin layer of carbon prior to loading into the SEM chamber. The samples were examined using an electron beam with an accelerating voltage of 20 kV and a beam current of 0.1 nA. Spectra were collected with an optimized period. Multiple points were examined in each phase within the sample. Compositional estimates were calculated using SEM Quant software to correct intensities for matrix effects.

Magnetic Measurements: The magnetization measurements were performed using a physical property measurement system (PPMS) Dynacool manufactured by Quantum Design, Inc., on pieces of  $EuCd_2Sb_2$  obtained under high pressure. The PPMS operates over a temperature range of 1.8-300 K and in applied fields of up to 90 kOe.

Resistance and Specific Heat Measurements: A four-probe method using platinum wires was applied for the resistance measurements on a piece of the high pressure sample. The aforementioned PPMS was used, employing the standard resistivity puck. The temperature and field dependent resistance was measured over a temperature range of 1.8–300 K and applied magnetic fields up to 9 T. Heat capacity measurements were done over temperatures of 2–80 K using Apiezon N-type grease without an applied magnetic field.

# **Supporting Information**

Supporting Information is available from the Wiley Online Library or from the author

# Acknowledgements

The work at Xie's group was supported by the U.S. DOE-Basic Energy Sciences under Contract DE-SC0023648. The work at Rutgers and BNL was supported by the US Department of Energy Office of Science Basic Energy Sciences as part of the Computational Materials Science Program. K.P.K and L.W acknowledge support by the U.S. Department of Energy (DOE), Office of Science, Office of Basic Energy Sciences, Division of Material Sciences and Engineering under award number 10122.

#### **Conflict of Interest**

The authors declare no conflict of interest.

## **Data Availability Statement**

The data that support the findings of this study are available from the corresponding author upon reasonable request.

### **Keywords**

DFT calculation, high pressure high temperature synthesis, Kondo insulator

Received: March 31, 2023 Revised: April 28, 2023 Published online:

- [1] J. E. Moore, Nature 2010, 464, 194.
- [2] Y. L. Chen, J.-H. Chu, J. G. Analytis, Z. K. Liu, K. Igarashi, H.-H. Kuo, X. L. Qi, S. K. Mo, R. G. Moore, D. H. Lu, M. Hashimoto, T. Sasagawa, S. C. Zhang, I. R. Fisher, Z. Hussain, Z. X. Shen, *Science* 2010, 329, 659.

- [3] S. Borisenko, D. Evtushinsky, Q. Gibson, A. Yaresko, K. Koepernik, T. Kim, M. Ali, J. van den Brink, M. Hoesch, A. Fedorov, E. Haubold, Y. Kushnirenko, I. Soldatov, R. Schäfer, R. J. Cava, Nat. Commun. 2019, 10, 3424.
- [4] M. M. Otrokov, I. I. Klimovskikh, H. Bentmann, D. Estyunin, A. Zeugner, Z. S. Aliev, S. Gaß, A. U. B. Wolter, A. V. Koroleva, A. M. Shikin, M. Blanco-Rey, M. Hoffmann, I. P. Rusinov, A. Y. Vyazovskaya, S. V. Eremeev, Y.u. M. Koroteev, V. M. Kuznetsov, F. Freyse, J. Sánchez-Barriga, I. R. Amiraslanov, M. B. Babanly, N. T. Mamedov, N. A. Abdullayev, V. N. Zverev, A. Alfonsov, V. Kataev, B. Büchner, E. F. Schwier, S. Kumar, A. Kimura, et al., Nature 2019, 576, 416.
- [5] D. Zhang, M. Shi, T. Zhu, D. Xing, H. Zhang, J. Wang, Phys. Rev. Lett. 2019, 122, 206401.
- [6] I. I. Klimovskikh, M. M. Otrokov, D. Estyunin, S. V. Eremeev, S. O. Filnov, A. Koroleva, E. Shevchenko, V. Voroshnin, A. G. Rybkin, I. P. Rusinov, M. Blanco-Rey, M. Hoffmann, Z. S. Aliev, M. B. Babanly, I. R. Amiraslanov, N. A. Abdullayev, V. N. Zverev, A. Kimura, O. E. Tereshchenko, K. A. Kokh, L. Petaccia, G. Di Santo, A. Ernst, P. M. Echenique, N. T. Mamedov, A. M. Shikin, E. V. Chulkov, npj Quantum Mater. 2020, 5, 54.
- [7] J. Li, Y. Li, S. Du, Z. Wang, B.-L. Gu, S.-C. Zhang, K. He, W. Duan, Y. Xu, Sci. Adv. 2019, 5, eaaw5685.
- [8] G. Hua, S. Nie, Z. Song, R. Yu, G. Xu, K. Yao, Phys. Rev. B 2018, 98, 201116.
- [9] N. H. Jo, B. Kuthanazhi, Y. Wu, E. Timmons, T.-H. Kim, L. Zhou, L.-L. Wang, B. G. Ueland, A. Palasyuk, D. H. Ryan, R. J. McQueeney, K. Lee, B. Schrunk, A. A. Burkov, R. Prozorov, S. L. Bud'ko, A. Kaminski, P. C. Canfield, *Phys. Rev. B* **2020**, *101*, 140402.
- [10] L.-L. Wang, N. H. Jo, B. Kuthanazhi, Y. Wu, R. J. McQueeney, A. Kaminski, P. C. Canfield, Phys. Rev. B 2019, 99, 245147.
- [11] A. M. Goforth, P. Klavins, J. C. Fettinger, S. M. Kauzlarich, *Inorg. Chem.* 2008, 47, 11048.
- [12] A. F. May, M. A. McGuire, D. J. Singh, J. Ma, O. Delaire, A. Huq, W. Cai, H. Wang, *Phys. Rev. B* 2012, 85, 035202.
- [13] S. Pakhira, M. A. Tanatar, D. C. Johnston, Phys. Rev. B 2020, 101, 214407
- [14] A. C. Payne, A. E. Sprauve, M. M. Olmstead, S. M. Kauzlarich, J. Y. Chan, B. A. Reisner, J. W. Lynn, J. Solid State Chem. 2002, 163, 498.
- [15] H. Su, B. Gong, W. Shi, H. Yang, H. Wang, W. Xia, Z. Yu, P. J. Guo, J. Wang, L. Ding, L. Xu, X. Li, X. Wang, Z. Zou, N. Yu, Z. Zhu, Y. Chen, Z. Liu, K. Liu, G. Li, Y. Guo, APL Mater. 2020, 8, 011109.
- [16] A. Artmann, A. Mewis, M. Roepke, G. Michels, Z. Anorg. Allg. Chem. 1996, 622, 679.
- [17] B. Q. Lv, H. M. Weng, B. B. Fu, X. P. Wang, H. Miao, J. Ma, P. Richard, X. C. Huang, L. X. Zhao, G. F. Chen, Z. Fang, X. Dai, T. Qian, H. Ding, *Phys. Rev. X* 2015, 5, 031013.
- [18] S.-M. Huang, S.-Y. Xu, I. Belopolski, C.-C. Lee, G. Chang, B. Wang, N. Alidoust, G. Bian, M. Neupane, C. Zhang, S. Jia, A. Bansil, H. Lin, M. Z. Hasan, *Nat. Commun.* 2015, 6, 7373.
- [19] B. Q. Lv, N. Xu, H. M. Weng, J. Z. Ma, P. Richard, X. C. Huang, L. X. Zhao, G. F. Chen, C. E. Matt, F. Bisti, V. N. Strocov, J. Mesot, Z. Fang, X. Dai, T. Qian, M. Shi, H. Ding, Nat. Phys. 2015, 11, 724.
- [20] H. Weng, C. Fang, Z. Fang, B. A. Bernevig, X. Dai, Phys. Rev. X 2015, 5. 011029.
- [21] M. N. Ali, J. Xiong, S. Flynn, J. Tao, Q. D. Gibson, L. M. Schoop, T. Liang, N. Haldolaarachchige, M. Hirschberger, N. P. Ong, R. J. Cava, *Nature* 2014, 514, 205.
- [22] A. A. Soluyanov, D. Gresch, Z. Wang, Q. Wu, M. Troyer, X. Dai, B. A. Bernevig, *Nature* 2015, 527, 495.
- [23] T.-R. Chang, S.-Y. Xu, G. Chang, C.-C. Lee, S.-M. Huang, B. Wang, G. Bian, H. Zheng, D. S. Sanchez, I. Belopolski, N. Alidoust, M. Neupane, A. Bansil, H.-T. Jeng, H. Lin, M. Z. Hasan, *Nat. Commun.* 2016, 7, 10639.
- [24] Y. Wu, D. Mou, N. H. Jo, K. Sun, L. Huang, S. L. Bud'ko, P. C. Canfield, A. Kaminski, *Phys. Rev. B* **2016**, *94*, 121113.

**ADVANCED** SCIENCE NEWS ADVANCED FUNCTIONA MATERIALS

www.advancedsciencenews.com

www.afm-journal.de

- [25] K. Deng, G. Wan, P. Deng, K. Zhang, S. Ding, E. Wang, M. Yan, H. Huang, H. Zhang, Z. Xu, J. Denlinger, A. Fedorov, H. Yang, W. Duan, H. Yao, Y. Wu, S. Fan, H. Zhang, X. Chen, S. Zhou, *Nat. Phys.* 2016, 12, 1105.
- [26] Z. Wang, D. Gresch, A. A. Soluyanov, W. Xie, S. Kushwaha, X. Dai, M. Troyer, R. J. Cava, B. A. Bernevig, Phys. Rev. Lett. 2016, 117, 056805.
- [27] E. V. Sampathkumaran, L. C. Gupta, R. Vijayaraghavan, K. V. Gopalakrishnan, R. G. Pillay, H. G. Devare, J. Phys. C: Solid State Phys. 1981, 14, L237.
- [28] X. Gui, G. J. Finkelstein, K. Chen, T. Yong, P. Dera, J. Cheng, W. Xie, Inorg. Chem. 2019, 58, 8933.
- [29] S. K. Dhar, P. Manfrinetti, A. Palenzona, J. Alloys Compd. 1997, 252, 24.
- [30] R. Movshovich, M. Jaime, J. D. Thompson, C. Petrovic, Z. Fisk, P. G. Pagliuso, J. L. Sarrao, Phys. Rev. Lett. 2001, 86, 5152.
- [31] K. M. Stadler, Z. P. Yin, J. von Delft, G. Kotliar, A. Weichselbaum, Phys. Rev. Lett. 2015, 115, 136401.
- [32] R. Adlerm, A. Kutepov, G. Kotliar, Bringing Electronic Structure Codes into the Modern Software Ecosystem, APS MArch Meeting 2019.
- [33] D. Walker, J. Li, Matter Radiat. Extremes 2020, 5, 018402.